ACS APPLIED OPTICAL MATERIALS

pubs.acs.org/acsaom

Article

Enhancing Magnetic Dipole Emission from 2D Hybrid Organic−Inorganic Perovskites via Mie Resonator Dimers

Roark Chao, Larry K. Heki, Wesley K. Mills, and Jon A. Schuller*

Cite This: ACS Appl. Opt. Mater. 2025, 3, 737−742

Read Online

ACCESS | Metrics & More | Article Recommendations | Supporting Information

ABSTRACT: Recently, layered 2D hybrid organic−inorganic perovskites (HOIPs) like butylammonium lead iodide (BA_2PbI_4) have been shown to exhibit ultrabright out-of-plane-oriented magnetic dipole (MD_{OP}) photoluminescence (PL) arising from self-trapped excitons (STEs). The MD_{OP} emission, however, has considerable spectral overlap with the dominant in-plane-oriented electric dipole (ED_{IP}) transitions, making it difficult to interrogate STE properties. Here, we theoretically investigate opportunities to use Mie resonator dimers to selectively enhance the MD_{OP} emission through the Purcell effect. We calculate relative MD and ED Purcell enhancements at dimer center as well as average values across the dimer geometry. We show that the selective enhancement is excellent at the dimer center enabling nearly pure MD_{OP} emission (96%) at the MD emission peak (540 nm) as well as predominant MD_{OP} emission (up to 77%) across the entire integrated spectrum (500−600 nm). We subsequently show, however, that away from the dimer center, Purcell enhancement of the relatively weak out-of-plane ED_{OP} transitions competes with MD_{OP} enhancements, reducing the branching ratio (73% at the MD emission peak, 39% spectrally integrated). Lastly, we calculate how the Mie resonator dimer modifies the PL spectra and emitter radiation pattern. Notably, for volume-averaged dipoles, both MD and ED emissions are mediated via the dimer, producing a single donut-beam-like radiation pattern across the entire emission spectrum. Our results clarify the potential for achieving "pure" MD emission from 2D HOIPs via simple Mie resonator Purcell enhancements and highlight the importance of designing nanophotonic structures that can maintain desired selective enhancements away from high-symmetry points.

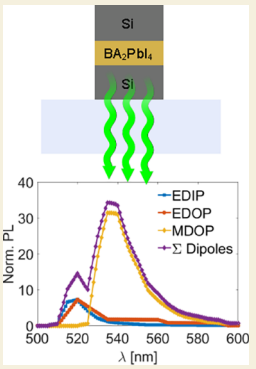

KEYWORDS: *magnetic dipole, optical transitions, perovskites, photoluminescence enhancement, resonator metasurfaces, Mie resonance*

INTRODUCTION

Electric dipole (ED) transitions dominate luminescent light-matter interactions as higher order magnetic dipole (MD) transitions are either very weak (as in atomic systems) or forbidden via selection rules (as in nearly all semiconductors).[1] Accordingly, extensive research on enhancing photoluminescent Purcell enhancements via, e.g., photonic crystals,[2−4] Mie resonators,[5−10] metamaterials,[11−13] and metasurfaces[14−17] primarily focuses on enhancing ED emission rates. In general, an emitter embedded within one of these systems experiences localized field enhancements that result in a higher ratio of radiated power by the system than the power radiated in a homogeneous medium ($\frac{P_{rad}}{P_{0,rad}}$) − an effect quantified by the Purcell factor F_{dip} of the emitter.[1,18]

In contrast with traditional ED emitters, the advent of artificial optical magnetism in metamaterials[19−22] and Mie resonators[23−27] has led to renewed interest in the visible and infrared intra-$4f^n$ MD transitions of lanthanide ions.[28−30] Recent literature has explored a variety of ways to use these MD transitions to, e.g., probe localized magnetic fields[31,32] and create negative index metamaterials.[33,34] From this renewed interest, demonstrated approaches for enhancing MD emission[35,36] include plasmonic antennas,[37−42] Mie resonators,[43−49] and metasurfaces.[50−54]

More recently, ultrabright MD emission was discovered in a wide class of two-dimensional Ruddlesden−Popper phase hybrid organic−inorganic perovskites (HOIP).[55] These transitions are thought to derive from self-trapped excitons and are 1000s of times stronger than the lanthanide MD transitions.[56] The strong MD transition rates, and the material's extended nature (i.e., not an atomic or ionic system), even lead to atomic-scale nonunity optical permeabilities.[57] However, approaches for enhancing the highly oriented MD emission in these materials have not yet been demonstrated.

A schematic molecular structure of the 2D HOIP butylammonium lead iodide (BA_2PbI_4) is shown in Figure 1A. The structure consists of alternating sheets of atomically thick inorganic octahedra separated via organic butylammo-

Received: December 23, 2024
Revised: February 20, 2025
Accepted: March 10, 2025
Published: March 14, 2025

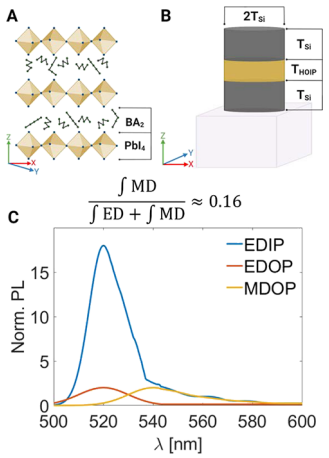

Figure 1. A) Schematic of the resonator metasurface. The silicon layers maintain isotropic scaling for their radii and thicknesses as described by T_{Si}, with the BA_2PbI_4 HOIP layer having a varied thickness of T_{HOIP}. B) Schematic of the crystal structure of BA_2PbI_4 showcasing the vertically layered alternating structure. C) Plot of the normalized photoluminescence per emission wavelength showcasing strong MDOP contribution, as demonstrated in prior works.[55]

nium cations. As such, the material behaves like an assembly of noninteracting 2D quantum wells, with band-edge optical transitions deriving from the inorganic layers. Unlike the lanthanide ions, the system is highly anisotropic, leading to highly anisotropic optical properties.[58] For instance, the photoluminescence (reproduced with permission from ref 55.) primarily arises from in-plane oriented ED transitions (ED_{IP}, blue), with smaller contributions from out-of-plane oriented ED (ED_{OP}, red) and MD (MD_{OP}, green) transitions. Approximately 16% of the integrated photoluminescence derives from MD_{OP} transitions (i.e., branching ratio of 0.16). At the peak MD_{OP} emission wavelength (540 nm), the emission rate is roughly equal to that of the dominant ED_{IP} channel (i.e., branching ratio of 0.5). Thus, clearly distinguishing ED and MD properties is challenging, and typically requires high-NA (NA > 1) momentum-resolved measurement techniques that are incompatible with, e.g., low-temperature measurements, nontransparent substrates, etc. Achieving sufficiently large MD Purcell enhancements could enable direct studies of the MD emission from self-trapped excitons (STEs) without the need for momentum-resolved measurements.

In this paper, we present a Mie resonator designed to selectively enhance the MD component of BA_2PbI_4 photoluminescence (PL). We first consider the high-symmetry position (i.e., the center of the dimer) to note a branching ratio of 96% at the 540 nm wavelength MD_{OP} emission peak. Then, we account for the 2D HOIP nature of BA_2PbI_4 by finding the volume-averaged branching ratio, which was determined to be 73% at the 540 nm wavelength MD_{OP} emission peak. Collectively, we demonstrate the promising future of HOIP-focused metasurfaces from which "pure" magnetic dipole emissions can be found.

RESULTS AND DISCUSSION

Similar to plasmonic dimers,[41,44] Mie resonator dimers enable large magnetic field enhancements[43−45] within gap regions via coupling effects. A schematic of the Mie resonator dimer studied here is shown in Figure 1B. The resonator comprises a BA_2PbI_4 layer sandwiched between two high refractive index crystalline silicon disks with identical radii and thicknesses (T_{Si}), placed on top of a SiO_2 substrate. Similar dimer structures were previously shown to support large H_z field enhancements when illuminated with appropriate beam symmetries.[59] Each dimer subelement (i.e., monomer) exhibits a fundamental H_z-oriented MD Mie resonance (Figure S1A-B, Supporting Information). By coupling two elements together, we form a dimer structure with a nearly identical resonance frequency and large field enhancements within the gap material (Figure S1C−D, Supporting Information). Our findings demonstrate strong out-of-plane magnetic field coupling and weak in-plane electric field coupling within the BA_2PbI_4 layer. We simulate the emission enhancement of oriented EDs and MDs with perfectly matched layers (PML) for *x*-, *y*-, and *z*-axis boundary conditions (Figure S2, Supporting Information). Purcell enhancements are calculated as the ratio of emitted power of oriented dipole emitters embedded within the structure divided by the emitted power of the same oriented dipole emitter in vacuum. The structure is oriented such that the *z*-axis is the OP orientation with the *x*- and *y*-axes defining the IP orientations. Owing to the rotational symmetry of the system, simulating a single in-plane dipole orientation (chosen to be the *x*-axis) is sufficient to describe ED_{IP} without loss of generality. For a range of BA_2PbI_4 layer thicknesses (10−60 nm), dimers with T_{Si} = 58 nm produce large 540 nm wavelength MD_{OP} Purcell enhancements in the dimer center (Figure 2A). Enhancements reach values as large as 18 for the thinnest BA_2PbI_4 layers and are larger than 3 for all simulated layer thicknesses. This dependence of Purcell enhancements on the dimer gap is commonly observed in other systems.

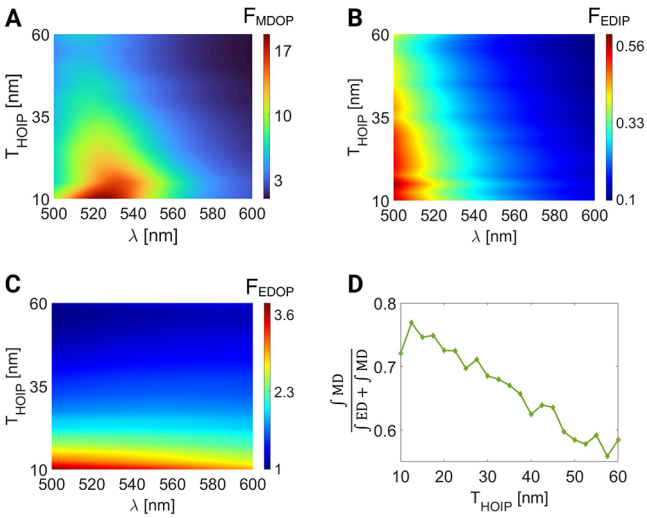

Figure 2. Simulated radiative Purcell factor due to centered A) MD_{OP}, B) ED_{IP}, and C) ED_{OP} as a function of wavelength and HOIP thickness. D) Weighted photoluminescence contribution from the MD_{OP} across the 100 nm wavelength spectrum as a function of HOIP thickness.

To determine how the branching ratio between oriented ED and MD emission channels (Figure 1C) is modified by interaction with the dimer nanoantenna, we perform similar simulations for ED_{IP} (Figure 2B) and ED_{OP} (Figure 2C). Emission from ED_{IP} is actually *suppressed* (F_{EDIP} < 1), for all layer thicknesses T_{HOIP}. ED_{OP} exhibits modest enhancements for the thinnest layers. As modified via these Purcell

https://doi.org/10.1021/acsaom.4c00529
ACS Appl. Opt. Mater. 2025, 3, 737−742

enhancements, the calculated wavelength-integrated MD branching ratio ($\frac{\int F_{MDOP} d\lambda}{\int F_{ED} d\lambda + \int F_{MDOP} d\lambda}$) is shown in Figure 2D. The best overall MD enhancement is observed for T_{HOIP} = 12.5 nm, where MD_{OP} accounts for ∼ 77% of the total photoluminescence intensity across all emission wavelengths. The relative predominance of MD_{OP} at the 540 nm MD_{OP} emission peak is even greater, with 96% of the PL at this wavelength arising through the MD_{OP} emission channel.

Unlike MD emission from, e.g., Lanthanide ions, which behave as point sources, MD emission from 2D HOIPs necessarily occurs across an extended material. Therefore, it is imperative to consider how the different Purcell factors vary for emission away from the high-symmetry resonator center. The radiative Purcell factor for oriented dipoles at various positions away from the resonator center are plotted in Figure 3. Given

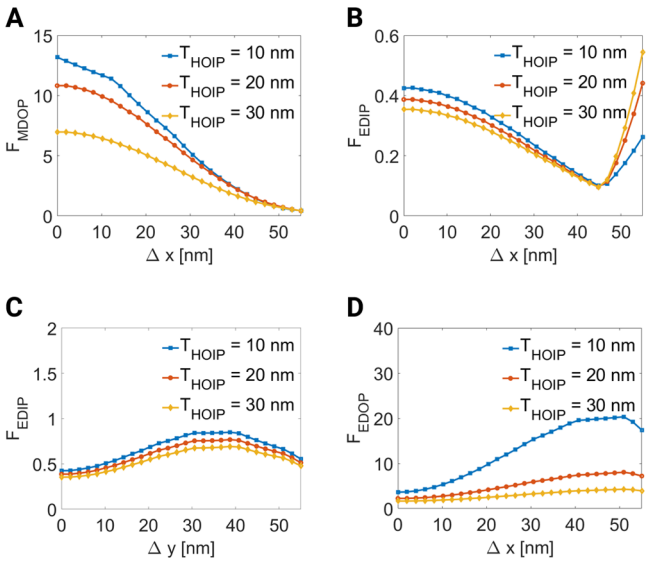

Figure 3. A) Simulated MD_{OP} radiative Purcell factor at 540 nm as the MD_{OP} is moved away from the center along the *x*-axis. Simulated *x*-polarized ED_{IP} radiative Purcell factor at 520 nm as the ED_{IP} is moved away from the center along the B) *x*-axis and C) *y*-axis. D) Simulated ED_{OP} radiative Purcell factor at 520 nm as the ED_{OP} is moved away from the center along the *x*-axis.

the system's cylindrical symmetry, a single direction (*x*-axis here) fully describes the system for MD_{OP} (Figure 3A) and ED_{OP} (Figure 3D). For ED_{IP}, on the other hand, we must consider shifts both parallel (*x*-axis) and perpendicular (*y*-axis) to the dipole orientation (Figures 3B,C). MD_{OP} enhancement decreases away from resonator center (Figure 3A) whereas ED_{OP} enhancement increases (Figure 3D). Although ED_{IP} enhancements also vary across the resonator, the values remain modest.

To understand the *overall* enhancement, we calculate the average Purcell factor for dipoles distributed evenly across the entire resonator geometry (Figure S3, Supporting Information.) The average Purcell factors for MD_{OP}, ED_{IP}, and ED_{OP} are shown in Figures 4A-C, respectively. Relative to the high-symmetry center, the average enhancement for MD_{OP} is reduced while the average enhancement for ED_{OP} is increased. As a result, the wavelength integrated MDOP branching ratio peaks at a value of ∼ 39% (Figure 4D). At 540 nm, the MDOP branching ratio reaches a value of 73%.

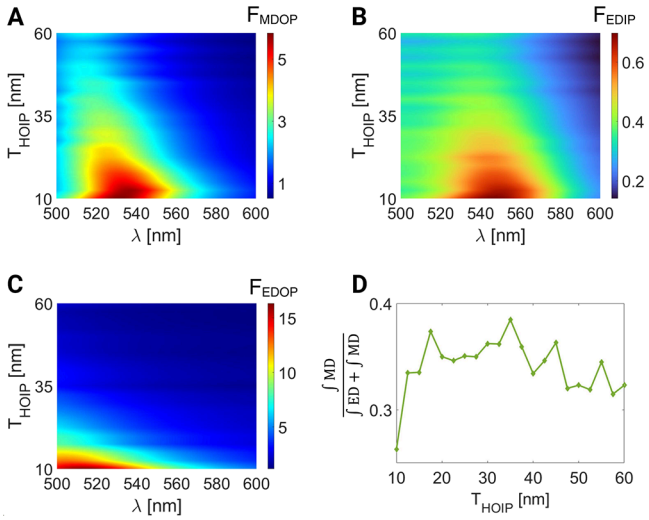

Figure 4. Simulated radiative Purcell factor due to averaged A) MD_{OP}, B) ED_{IP}, and C) ED_{OP} as a function of wavelength and HOIP thickness. D) Weighted photoluminescence contribution from the MD_{OP} across the 100 nm wavelength spectrum as a function of HOIP thickness.

Lastly, we summarize the effect of Purcell enhancements on the emission spectra and radiation patterns for both centered dipoles with T_{HOIP} = 12.5 nm (Figure 5A) and volume-averaged dipoles with T_{HOIP} = 35 nm (Figure 5B), respectively. For centered dipoles, the 540 nm MDOP emission peak becomes the predominant spectral feature. For volume-averaged dipoles, the 520 nm ED emission remains the predominant spectral feature while the MD sideband becomes

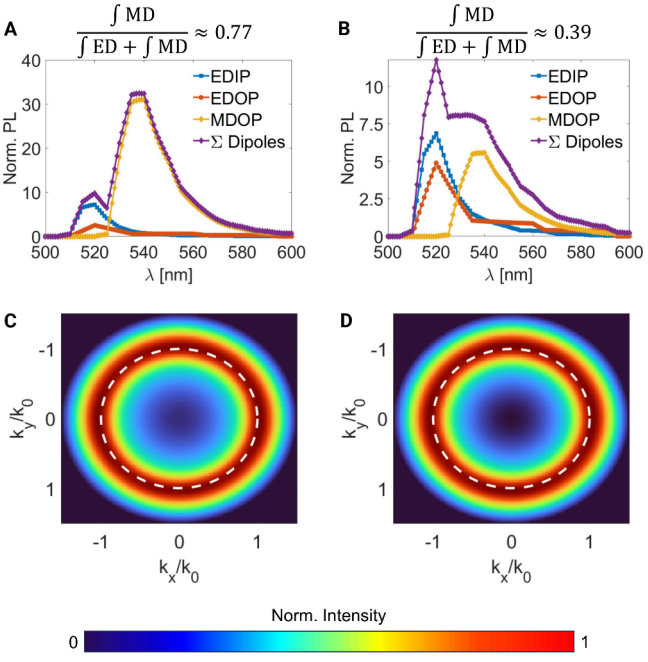

Figure 5. Simulated ED_{IP}, ED_{OP}, and MD_{OP} weights for A) centralized dipoles with T_{HOIP} = 12.5 nm and B) averaged dipoles with T_{HOIP} = 35 nm. MD_{OP} contribution across this spectrum is ∼ 77% and ∼ 39%, respectively. Simulated total momentum-resolved emission pattern at C) 520 nm and D) 540 nm generated by volume averaged dipoles. Dotted lines represent the critical angle for panels C–D.

https://doi.org/10.1021/acsaom.4c00529
ACS Appl. Opt. Mater. 2025, 3, 737–742

much more pronounced relative to the original values (Figure 1C), enabling a wavelength-dependent branching ratio of 39%. Interestingly, the simulated radiation patterns exhibit a marked difference from the original situation (Figure S4A-D, Supporting Information). The emission from all three possible dipole sources is mediated through the resonator producing a magnetic dipole-driven donut beam radiation pattern that is nearly identical across different emission wavelengths (Figures 5C−D).

CONCLUSION

We used FDTD simulations to design and analyze an optical frequency Mie resonator capable of enhancing magnetic dipole transitions while simultaneously reducing electric dipole transitions. We show the photoluminescence generated within a hybrid organic−inorganic perovskite, like butylammonium lead iodide, can be tailored to be dominated by the magnetic dipole when considering centered emissions. Taking into account volume-averaged emission, we observe near-equal wavelength-integrated contributions from magnetic and electric dipoles due to the enhancement of ED_{OP} away from resonator center. The emission at 540 nm, however, arises predominantly (>73%) from MD_{OP}. Our work establishes nanophotonic approaches for selectively enhancing the magnetic dipole emission from STEs in 2D HOIPs, laying the groundwork for future studies where the properties of these specific excitons are interrogated without the need for momentum-resolved experimentation and analyses.

METHODOLOGY

3D dipole simulations were performed using Ansys Lumerical FDTD. PML boundary conditions were used along all axes, with a 32-layer, steep-angle PML boundary used along the *z*-axis. An override mesh was used in the HOIP region with 1 nm resolution along the *z*-axis and 5 nm resolution along the *x*- and *y*-axes. Purcell factors were simulated by enclosing the meta-element with power monitors in 3D space assuming dipoles emit at their resonant wavelengths. Momentum space patterns were simulated using a far field projection monitor spanning 10 wavelengths with 5 nm override meshing along the *x*- and *y*-axes placed directly underneath the Mie resonator at the top of the SiO_2 substrate with a 1 nm override mesh along the *z*-axis.

ASSOCIATED CONTENT

Supporting Information

The Supporting Information is available free of charge at https://pubs.acs.org/doi/10.1021/acsaom.4c00529.

Additional details regarding the resonator mode profiles, simulation setup, calculation of the volumetric average, and thin-film momentum space patterns (PDF)

AUTHOR INFORMATION

Corresponding Author

Jon A. Schuller − *Department of Electrical and Computer Engineering, University of California, Santa Barbara, California 93106, United States;* orcid.org/0000-0001-6949-3569; Email: jonschuller@ece.ucsb.edu

Authors

Roark Chao − *Department of Electrical and Computer Engineering, University of California, Santa Barbara, California 93106, United States;* orcid.org/0009-0001-3267-5956

Larry K. Heki − *Materials Department, University of California, Santa Barbara, California 93106, United States*

Wesley K. Mills − *Department of Electrical and Computer Engineering, University of California, Santa Barbara, California 93106, United States;* orcid.org/0000-0003-1188-2056

Complete contact information is available at: https://pubs.acs.org/10.1021/acsaom.4c00529

Notes

The authors declare no competing financial interest.

ACKNOWLEDGMENTS

The authors would like to thank Y. Nemoto, E. J. Rumbos-Perez, and A. J. Walburg for their helpful discussions. This work was primarily supported by the Office of Naval Research (Grant No. N00014-22-1-2337). Partial funding came from the Gene and Susan Lucas Undergraduate Research Fund, as well as the Undergraduate Research and Creative Activities Grant from the University of California, Santa Barbara. Numerical calculations were performed with support from computational facilities purchased with funds from the National Science Foundation (CNS-1725797) and administered by the Center for Scientific Computing (CSC). The CSC is supported by the California NanoSystems Institute and the Materials Research Science and Engineering Center (MRSEC; NSF DMR 2308708) at UC Santa Barbara. Figures were created using BioRender.com.

REFERENCES

(1) Novotny, L.; Hecht, B. *Principles of Nano-Optics*; Cambridge University Press, 2012.

(2) Joannopoulos, J. D.; Villeneuve, P. R.; Fan, S. Photonic Crystals. *Solid State Commun.* **1997**, *102* (2), 165−173.

(3) Busch, K.; Vats, N.; John, S.; Sanders, B. C. Radiating Dipoles in Photonic Crystals. *Phys. Rev. E* **2000**, *62* (3), 4251−4260.

(4) Lousse, V.; Vigneron, J.-P.; Bouju, X.; Vigoureux, J.-M. Atomic Radiation Rates in Photonic Crystals. *Phys. Rev. B* **2001**, *64* (20), No. 201104.

(5) Liu, T.; Xu, R.; Yu, P.; Wang, Z.; Takahara, J. Multipole and Multimode Engineering in Mie Resonance-Based Metastructures. *Nanophotonics* **2020**, *9* (5), 1115−1137.

(6) Tonkaev, P.; Kivshar, Yu. High-Q Dielectric Mie-Resonant Nanostructures (Brief Review). *Jetp Lett.* **2020**, *112* (10), 615−622.

(7) Alhalaby, H.; Zaraket, H.; Principe, M. Enhanced Photoluminescence with Dielectric Nanostructures: A Review. *Results in Optics* **2021**, *3*, No. 100073.

(8) Ahamad, M. A.; Ahmed Inam, F. Electromagnetic Scattering Controlled All-Dielectric Cavity-Antenna for Bright, Directional, and Purely Radiative Single-Photon Emission. *J. Appl. Phys.* **2024**, *136* (8), No. 083104.

(9) Babicheva, V. E.; Evlyukhin, A. B. Mie-Resonant Metaphotonics. *Adv. Opt. Photon., AOP* **2024**, *16* (3), 539−658.

(10) Rybin, M. V.; Kivshar, Y. Metaphotonics with Subwavelength Dielectric Resonators. *npj Nanophoton.* **2024**, *1* (1), 1−8.

(11) Poddubny, A. N.; Belov, P. A.; Ginzburg, P.; Zayats, A. V.; Kivshar, Y. S. Microscopic Model of Purcell Enhancement in Hyperbolic Metamaterials. *Phys. Rev. B* **2012**, *86* (3), No. 035148.

(12) Chebykin, A. V.; Orlov, A. A.; Shalin, A. S.; Poddubny, A. N.; Belov, P. A. Strong Purcell Effect in Anisotropic ϵ-near-Zero Metamaterials. *Phys. Rev. B* **2015**, *91* (20), No. 205126.
(13) Monticone, F.; Alù, A. Metamaterial, Plasmonic and Nanophotonic Devices. *Rep. Prog. Phys.* **2017**, *80* (3), No. 036401.
(14) Kippenberg, T. J.; Tchebotareva, A. L.; Kalkman, J.; Polman, A.; Vahala, K. J. Purcell-Factor-Enhanced Scattering from Si Nanocrystals in an Optical Microcavity. *Phys. Rev. Lett.* **2009**, *103* (2), No. 027406.
(15) Krasnok, A.; Glybovski, S.; Petrov, M.; Makarov, S.; Savelev, R.; Belov, P.; Simovski, C.; Kivshar, Y. Demonstration of the Enhanced Purcell Factor in All-Dielectric Structures. *Appl. Phys. Lett.* **2016**, *108* (21), No. 211105.
(16) Staude, I.; Pertsch, T.; Kivshar, Y. S. All-Dielectric Resonant Meta-Optics Lightens Up. *ACS Photonics* **2019**, *6* (4), 802−814.
(17) Vaskin, A.; Kolkowski, R.; Koenderink, A. F.; Staude, I. Light-Emitting Metasurfaces. *Nanophotonics* **2019**, *8* (7), 1151−1198.
(18) Krasnok, A. E.; Slobozhanyuk, A. P.; Simovski, C. R.; Tretyakov, S. A.; Poddubny, A. N.; Miroshnichenko, A. E.; Kivshar, Y. S.; Belov, P. A. An Antenna Model for the Purcell Effect. *Sci. Rep.* **2015**, *5* (1), 12956.
(19) Smith, D. R.; Padilla, W. J.; Vier, D. C.; Nemat-Nasser, S. C.; Schultz, S. Composite Medium with Simultaneously Negative Permeability and Permittivity. *Phys. Rev. Lett.* **2000**, *84* (18), 4184−4187.
(20) Grigorenko, A. N.; Geim, A. K.; Gleeson, H. F.; Zhang, Y.; Firsov, A. A.; Khrushchev, I. Y.; Petrovic, J. Nanofabricated Media with Negative Permeability at Visible Frequencies. *Nature* **2005**, *438* (7066), 335−338.
(21) Monticone, F.; Alù, A. The Quest for Optical Magnetism: From Split-Ring Resonators to Plasmonic Nanoparticles and Nanoclusters. *J. Mater. Chem. C* **2014**, *2* (43), 9059−9072.
(22) Papadakis, G. T.; Fleischman, D.; Davoyan, A.; Yeh, P.; Atwater, H. A. Optical Magnetism in Planar Metamaterial Heterostructures. *Nat. Commun.* **2018**, *9* (1), 296.
(23) Schuller, J. A.; Zia, R.; Taubner, T.; Brongersma, M. L. Dielectric Metamaterials Based on Electric and Magnetic Resonances of Silicon Carbide Particles. *Phys. Rev. Lett.* **2007**, *99* (10), No. 107401.
(24) Zhao, Q.; Zhou, J.; Zhang, F.; Lippens, D. Mie Resonance-Based Dielectric Metamaterials. *Mater. Today* **2009**, *12* (12), 60−69.
(25) Ginn, J.; Brener, I.; Peters, D.; Wendt, J.; Stevens, J.; Hines, P.; Basilio, L.; Warne, L.; Ihlefeld, J.; Clem, P.; Sinclair, M. Realizing Optical Magnetism from Dielectric Metamaterials. *Physical review letters* **2012**, *108*, No. 097402.
(26) Kuznetsov, A. I.; Miroshnichenko, A. E.; Fu, Y. H.; Zhang, J.; Luk'yanchuk, B. Magnetic Light. *Sci. Rep* **2012**, *2* (1), 492.
(27) Kuznetsov, A. I.; Miroshnichenko, A. E.; Brongersma, M. L.; Kivshar, Y. S.; Luk'yanchuk, B. Optically Resonant Dielectric Nanostructures. *Science* **2016**, *354* (6314), aag2472.
(28) Freed, S.; Weissman, S. I. Multiple Nature of Elementary Sources of Radiation—Wide-Angle Interference. *Phys. Rev.* **1941**, *60* (6), 440−442.
(29) Drexhage, K. H. IV Interaction of Light with Monomolecular Dye Layers. In *Progress in Optics*; Wolf, E., Ed.; Elsevier, 1974; Vol. *12*, pp 163−232. .
(30) Dodson, C. M.; Zia, R. Magnetic Dipole and Electric Quadrupole Transitions in the Trivalent Lanthanide Series: Calculated Emission Rates and Oscillator Strengths. *Phys. Rev. B* **2012**, *86* (12), No. 125102.
(31) Noginova, N.; Zhu, G.; Mavy, M.; Noginov, M. A. Magnetic Dipole Based Systems for Probing Optical Magnetism. *J. Appl. Phys.* **2008**, *103* (7), No. 07E901.
(32) Taminiau, T. H.; Karaveli, S.; van Hulst, N. F.; Zia, R. Quantifying the Magnetic Nature of Light Emission. *Nat. Commun.* **2012**, *3* (1), 979.
(33) Thommen, Q.; Mandel, P. Left-Handed Properties of Erbium-Doped Crystals. *Opt. Lett., OL* **2006**, *31* (12), 1803−1805.
(34) Klar, T. A.; Kildishev, A. V.; Drachev, V. P.; Shalaev, V. M. Negative-Index Metamaterials: Going Optical. *IEEE J. Sel. Top. Quantum Electron.* **2006**, *12* (6), 1106−1115.
(35) Baranov, D. G.; Savelev, R. S.; Li, S. V.; Krasnok, A. E.; Alù, A. Modifying Magnetic Dipole Spontaneous Emission with Nanophotonic Structures. *Laser & Photonics Reviews* **2017**, *11* (3), No. 1600268.
(36) Calandrini, E.; Cerea, A.; De Angelis, F.; Zaccaria, R. P.; Toma, A. Magnetic Hot-Spot Generation at Optical Frequencies: From Plasmonic Metamolecules to All-Dielectric Nanoclusters. *Nanophotonics* **2019**, *8* (1), 45−62.
(37) Karaveli, S.; Weinstein, A. J.; Zia, R. Direct Modulation of Lanthanide Emission at Sub-Lifetime Scales. *Nano Lett.* **2013**, *13* (5), 2264−2269.
(38) Hein, S. M.; Giessen, H. Tailoring Magnetic Dipole Emission with Plasmonic Split-Ring Resonators. *Phys. Rev. Lett.* **2013**, *111* (2), No. 026803.
(39) Aigouy, L.; Cazé, A.; Gredin, P.; Mortier, M.; Carminati, R. Mapping and Quantifying Electric and Magnetic Dipole Luminescence at the Nanoscale. *Phys. Rev. Lett.* **2014**, *113* (7), No. 076101.
(40) Hussain, R.; Kruk, S. S.; Bonner, C. E.; Noginov, M. A.; Staude, I.; Kivshar, Y. S.; Noginova, N.; Neshev, D. N. Enhancing Eu^{3+} Magnetic Dipole Emission by Resonant Plasmonic Nanostructures. *Opt. Lett., OL* **2015**, *40* (8), 1659−1662.
(41) Mivelle, M.; Grosjean, T.; Burr, G. W.; Fischer, U. C.; Garcia-Parajo, M. F. Strong Modification of Magnetic Dipole Emission through Diabolo Nanoantennas. *ACS Photonics* **2015**, *2* (8), 1071−1076.
(42) Choi, B.; Iwanaga, M.; Sugimoto, Y.; Sakoda, K.; Miyazaki, H. T. Selective Plasmonic Enhancement of Electric- and Magnetic-Dipole Radiations of Er Ions. *Nano Lett.* **2016**, *16* (8), 5191−5196.
(43) Rolly, B.; Bebey, B.; Bidault, S.; Stout, B.; Bonod, N. Promoting Magnetic Dipolar Transition in Trivalent Lanthanide Ions with Lossless Mie Resonances. *Phys. Rev. B* **2012**, *85* (24), No. 245432.
(44) Baranov, D. G.; Savelev, R. S.; Li, S. V.; Krasnok, A. E.; Alù, A. Modifying Magnetic Dipole Spontaneous Emission with Nanophotonic Structures. *Laser & Photonics Reviews* **2017**, *11* (3), No. 1600268.
(45) Krasnok, A.; Caldarola, M.; Bonod, N.; Alú, A. Spectroscopy and Biosensing with Optically Resonant Dielectric Nanostructures. *Advanced Optical Materials* **2018**, *6* (5), No. 1701094.
(46) Sanz-Paz, M.; Ernandes, C.; Esparza, J. U.; Burr, G. W.; van Hulst, N. F.; Maitre, A.; Aigouy, L.; Gacoin, T.; Bonod, N.; Garcia-Parajo, M. F.; Bidault, S.; Mivelle, M. Enhancing Magnetic Light Emission with All-Dielectric Optical Nanoantennas. *Nano Lett.* **2018**, *18* (6), 3481−3487.
(47) Wiecha, P. R.; Majorel, C.; Girard, C.; Arbouet, A.; Masenelli, B.; Boisron, O.; Lecestre, A.; Larrieu, G.; Paillard, V.; Cuche, A. Enhancement of Electric and Magnetic Dipole Transition of Rare-Earth-Doped Thin Films Tailored by High-Index Dielectric Nanostructures. *Appl. Opt., AO* **2019**, *58* (7), 1682−1690.
(48) Bidault, S.; Mivelle, M.; Bonod, N. Dielectric Nanoantennas to Manipulate Solid-State Light Emission. *J. Appl. Phys.* **2019**, *126* (9), No. 094104.
(49) Dombi, P.; Pápa, Z.; Vogelsang, J.; Yalunin, S. V.; Sivis, M.; Herink, G.; Schäfer, S.; Groß, P.; Ropers, C.; Lienau, C. Strong-Field Nano-Optics. *Rev. Mod. Phys.* **2020**, *92* (2), No. 025003.
(50) Karaveli, S.; Zia, R. Strong Enhancement of Magnetic Dipole Emission in a Multilevel Electronic System. *Opt. Lett., OL* **2010**, *35* (20), 3318−3320.
(51) Vaskin, A.; Mashhadi, S.; Steinert, M.; Chong, K. E.; Keene, D.; Nanz, S.; Abass, A.; Rusak, E.; Choi, D.-Y.; Fernandez-Corbaton, I.; Pertsch, T.; Rockstuhl, C.; Noginov, M. A.; Kivshar, Y. S.; Neshev, D. N.; Noginova, N.; Staude, I. Manipulation of Magnetic Dipole Emission from Eu3+ with Mie-Resonant Dielectric Metasurfaces. *Nano Lett.* **2019**, *19* (2), 1015−1022.
(52) Abujetas, D. R.; Barreda, Á.; Moreno, F.; Sáenz, J. J.; Litman, A.; Geffrin, J.-M.; Sánchez-Gil, J. A. Brewster Quasi Bound States in

https://doi.org/10.1021/acsaom.4c00529
ACS Appl. Opt. Mater. 2025, 3, 737−742

the Continuum in All-Dielectric Metasurfaces from Single Magnetic-Dipole Resonance Meta-Atoms. *Sci. Rep* **2019**, *9* (1), 16048.
(53) Kalinic, B.; Cesca, T.; Balasa, I. G.; Trevisani, M.; Jacassi, A.; Maier, S. A.; Sapienza, R.; Mattei, G. Quasi-BIC Modes in All-Dielectric Slotted Nanoantennas for Enhanced Er3+ Emission. *ACS Photonics* **2023**, *10* (2), 534−543.
(54) Wu, L.; Huang, J.; Chen, D.; Fan, M.; Hu, M.; Zhou, C. Strong Purcell Effect of Magnetic Quasi-BICs in the Dielectric Metasurface. *New J. Phys.* **2023**, *25* (7), No. 073015.
(55) DeCrescent, R. A.; Venkatesan, N. R.; Dahlman, C. J.; Kennard, R. M.; Zhang, X.; Li, W.; Du, X.; Chabinyc, M. L.; Zia, R.; Schuller, J. A. Bright Magnetic Dipole Radiation from Two-Dimensional Lead-Halide Perovskites. *Sci. Adv.* **2020**, *6* (6), No. eaay4900.
(56) DeCrescent, R. A.; Du, X.; Kennard, R. M.; Venkatesan, N. R.; Dahlman, C. J.; Chabinyc, M. L.; Schuller, J. A. Even-Parity Self-Trapped Excitons Lead to Magnetic Dipole Radiation in Two-Dimensional Lead Halide Perovskites. *ACS Nano* **2020**, *14* (7), 8958−8968.
(57) DeCrescent, R. A.; Kennard, R. M.; Chabinyc, M. L.; Schuller, J. A. Optical-Frequency Magnetic Polarizability in a Layered Semiconductor. *Phys. Rev. Lett.* **2021**, *127* (17), No. 173604.
(58) DeCrescent, R. A.; Venkatesan, N. R.; Dahlman, C. J.; Kennard, R. M.; Chabinyc, M. L.; Schuller, J. A. Optical Constants and Effective-Medium Origins of Large Optical Anisotropies in Layered Hybrid Organic/Inorganic Perovskites. *ACS Nano* **2019**, *13* (9), 10745−10753.
(59) Das, T.; Schuller, J. A. Dark Modes and Field Enhancements in Dielectric Dimers Illuminated by Cylindrical Vector Beams. *Phys. Rev. B* **2017**, *95* (20), No. 201111.

https://doi.org/10.1021/acsaom.4c00529
ACS Appl. Opt. Mater. 2025, 3, 737−742